

A photometric imaging solar telescope, tunable in the extreme ultraviolet, utilizing multilayer x-ray optics

L. Golub, E. Deluca, P. Hamilton, and G. Nystrom

Smithsonian Astrophysical Observatory, 60 Garden Street, Cambridge, Massachusetts 02138

D. L. Windt^{a)}

Columbia Astrophysics Laboratory, 550 West 120th Street, New York, New York 10027

W. K. H. Schmidt and A. Dannenberg

Max-Planck-Institut für Aeronomie, Max-Planck-Str. 2, 37191 Katlenburg-Lindau, Germany

(Received 15 October 2001; accepted for publication 7 January 2002)

We present a new instrument for space-based observational solar physics, recently flown successfully on a sounding rocket, designed to provide high spatial resolution, time-resolved images of the solar corona at specific wavelengths in the extreme ultraviolet (XUV). The primary instrument employs multilayer x-ray mirrors in a novel geometry that affords quasi-monochromatic imaging at wavelengths tunable continuously over the spectral range from 17.1 to 21.1 nm. The secondary instrument also uses multilayer x-ray mirrors to provide high-resolution imaging at three fixed XUV wavelength bands. Both instruments use charge coupled device detectors and thin Al filters for rejection of unwanted wavelengths. We describe the design, construction, and performance of the instrument and discuss prospects for the future. © 2002 American Institute of Physics. [DOI: 10.1063/1.1453506]

I. INTRODUCTION

The past two decades of progress in instrumentation for solar physics, as well as developments in observational and analytical space-based studies, have led to a number of major satellite experiments, most notably the SoHO EIT¹ and TRACE.^{2,3} These two satellite instruments in particular, which have resulted in significant new understanding in the areas of coronal physics that they were designed to address, both make use of narrow-band multilayer x-ray mirrors to image the sun at specific wavelengths, corresponding to specific plasma temperatures, in the XUV band. The x-ray multilayer coatings, developed largely over the past 15 years, provide high-reflectance near normal-incidence, and thus make it possible to construct “conventional” telescopes (i.e., using normal-incidence mirrors, as is done routinely in the UV, optical, and IR parts of the spectra), in contrast to the traditional approach to astronomical x-ray and XUV telescopes that operate at grazing incidence, below the so-called “critical angle” for total external reflection where the x-ray reflectance is high. As a consequence of this new approach to x-ray telescope construction, the mirror substrates can be fabricated with better figure and finish control, thus leading to higher angular resolution and less scattering. (For example, the SoHO EIT and TRACE instruments have achieved angular resolutions of 5.0 and 1.0 arc sec, respectively). In addition, the intrinsic narrow-band response of the multilayer coatings acts as a wavelength filter, thus making it possible to produce quasi-monochromatic, high spatial resolution images of the coronal plasma.

The scientific achievements stemming from the success of these current solar missions have led to major questions that remain to be answered regarding coronal structuring, stability, and dynamics. To answer such questions will require simultaneous imaging and spectroscopy at even higher spatial resolution than has been achieved thus far, and over a more broad range of temperatures (i.e., over a more broad range of XUV wavelengths). For example, in order to explain the fundamental, though still-unresolved, problem of coronal heating, we will need to determine if there is fine structure in the corona beyond what has been resolved by TRACE. (Such fine structure has been suggested both by modeling and observational studies.^{4,5}) Also, because XUV coronal images taken in emission lines of the same element at only slightly different formation temperatures show very different structures, in general, the need for broad wavelength coverage is essential.

As part of our effort to develop the new instrumentation needed to address the current and future problems in solar coronal physics, we have built and recently flown on a sounding rocket the tunable XUV imager (TXI). The TXI instruments provide time- and temperature-resolved, high resolution imaging of the corona in a series of individual spectral lines. Unlike previous solar missions, however, the primary TXI instrument is tunable continuously over a range of XUV wavelengths, using a novel optical configuration utilizing multilayer x-ray optics. Additionally, the secondary TXI instrument employs narrow-band multilayer x-ray imagers, similar in function to those used in previous solar missions, but designed to operate at previously unexplored wavelengths. Apart from the technological goal of proving new instrumentation concepts that might be extended to future satellite missions, we also address the scientific objec-

^{a)}Electronic mail: windt@astro.columbia.edu

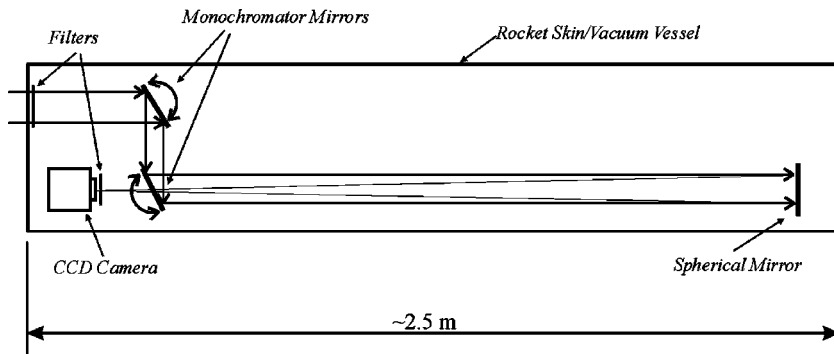


FIG. 1. Schematic diagram of the TXI sounding rocket instrument. The major components of the primary instrument are indicated. The secondary instrument, with its simple, prime-focus spherical telescope geometry, shares the optical bench with the primary instrument, but for clarity is not shown in this figure.

tive of more fully understanding the physics of the corona by observing all of the temperatures present in a specific range, and by viewing large spatial regions, corresponding to the scale size of dynamic coronal events, while studying the small scale instability and energy release sites in the low- β atmosphere (where β is the ratio of the gas to magnetic pressures) with time-resolved observations of density, temperature, and bulk motions (with velocity resolution of ~ 50 km/s) throughout the chromosphere, transition region, and corona.

In Sec. II we describe the instrumentation in detail, and in Sec. III we discuss the instrument performance, as determined both during calibration and flight. We discuss our results and prospects for the future in Sec. IV.

II. INSTRUMENT DESCRIPTION

The primary TXI instrument, shown schematically in Fig. 1, was designed to isolate a narrow coronal plasma temperature (i.e., wavelength) interval within a wide range of plasma temperatures, a performance requirement needed to overcome the daunting problems associated with observing the multitemperature corona.⁶ This performance is achieved by using a prime-focus, multilayer telescope mirror, having broadband wavelength response, in conjunction with a pair of flat multilayer mirrors having narrow-band wavelength response located in the incident beam of the telescope mirror, arranged as a Cowen-Golovchenko double-crystal monochromator.⁷ In this design, the two flat mirrors are mounted on perpendicularly oriented linear translation stages which intersect at the rotation axis of a rotary table; the mirrors are pulled against a precision linear bar so that a single motion, rotation of the table, causes the mirrors to both rotate to the desired incidence angles and simultaneously translate

so that the entrance and exit apertures of the system remain fixed. In this particular implementation, the flat mirrors operate at variable incidence angles of $45 \pm 12^\circ$; by varying these incidence angles the narrow bandpass of the system can be tuned continuously during flight over the range 17.1–21.1 nm. This wavelength band was selected because it includes a number of strong spectral lines spanning a wide range of plasma temperatures, ranging from O V ($\log T = 5.4$) to Fe XXIV ($\log T = 7.3$), as indicated in Table I.

The Cowen-type monochromator geometry used in the primary TXI instrument has the highly desirable property that there is no image motion in the focal plane during wavelength selection. The range of incidence angles ($45 \pm 12^\circ$) was selected as a performance compromise: at smaller incidence angles (i.e., closer to normal incidence), better spectral resolution can be achieved due to the response of the multilayer coatings (described below), but larger mirror motions are required to span a given wavelength band, and additionally the rapidly varying polarization sensitivity creates a difficult calibration problem; at larger incidence angles the angular size of the sun (0.5°) would cause wavelength mixing (due to the greater dispersion in the coatings at larger angles) which would effectively reduce the spectral resolution of the instrument.

The primary mirror is spherical, 13.5 cm in diameter, having a focal length of 2.2 m (thus achieving $f/20$, with a 10.8-cm-diameter aperture stop.) The two flat mirrors are rectangular (but with faceted corners) and measure 11.2×17.5 cm; the second flat mirror has an elliptical hole in its center (measuring 3.3×5.3 cm), to allow the converging beam from the sphere to reach the detector.

The three fused silica mirror substrates were fabricated by a commercial vendor (REO, Boulder, CO). The figure

TABLE I. Coronal emission lines in the TXI primary instrument spectral band and estimated exposure times.

Ion	Wavelength [nm]	Log T	Exposure time [s]
Fe IX	17.11	5.9	1.1
O V	17.22	5.4	10
O VI	17.29, 17.31	5.5	15
Fe X	17.45, 17.72	6.0	1.2
Fe XI	18.04	6.1	0.3
Fe XI	18.82	6.1	7
Fe XXIV	19.20	7.3	variable; flare line
Fe XII	19.24, 19.35, 19.51	6.2	0.6
Fe XIII	20.2, 20.38	6.2	2.5
Fe XIV	21.13	6.3	2.5

errors in the sphere were determined from optical interferometry to be <15 nm rms, while the flat mirrors were measured to be <10 nm rms; this surface figure is sufficient to meet the angular resolution goal of 1.0 arc sec. The surface finish of the mirrors was measured using atomic force microscopy and was found to be exceptionally small, 0.07 nm rms in all cases, as is needed to achieve low-scatter and high XUV reflectance.

X-ray multilayer coatings containing Mo and Si layers were deposited by magnetron sputtering on each of the three mirrors that comprise the primary TXI instrument, in a deposition system that has been described previously.⁸ To achieve broadband response on the primary mirror, that coating was designed with only 5 bilayers of Si(6.14 nm)/Mo(4.09 nm); under the reasonable assumption of 0.8 nm interface widths this design gives normal-incidence reflectance ranging from $\sim 5\%$ to 25% across the entire 17.1–21.1 nm wavelength band. In contrast, the narrow-band coatings on the flat mirrors were designed with 40 bilayers of Si(12.28 nm)/Mo(1.67 nm); the unusually small fraction of Mo (0.12) was chosen to reduce the width of the reflectance peak (at the expense of the peak height) in order to achieve the required spectral resolution of $\lambda/\Delta\lambda \sim 20$ (with $\Delta\lambda \sim 1$ nm) over the entire spectral band.

The secondary TXI instrument is designed to supplement the primary TXI instrument wavelength coverage and to provide a test bed for new multilayer coatings and observational wavelengths. The secondary instrument consists of three prime-focus spherical mirrors, 7.5 cm in diameter, also utilizing normal incidence multilayer coatings. These three mirrors share a separate imaging detector; passband selection is achieved during flight through the use of a rotating aperture plate located near the entrance aperture of the instrument. The focal length of each of these mirrors is also 2.2 m, and the design angular resolution is 2.0 arc sec. The fused silica mirror substrates were also fabricated commercially (REO) and were measured to have <10 nm rms figure and 0.07 nm rms finish. One of the three mirrors was coated with the same broadband multilayer film used on the sphere of the primary instrument; the other two mirrors use narrow-band multilayer structures containing either 40 bilayers of Si (9.79 nm)/Mo (1.21 nm), designed for response at $\lambda = 21.1$ nm (Fe XIV, $\log T = 6.3$) at normal incidence, or 40 bilayers of Si (11.78 nm)/Mo (1.46 nm), designed for use at $\lambda = 24.9$ nm (Ni XVII; $\log T = 6.5$). Again, as in the case of the two flat mirrors that comprise the monochromator used in the primary instrument, the unusually small fraction of Mo used in these latter two coatings was chosen intentionally to reduce the width of the reflectance peak in order to achieve the required spectral resolution.

Images are acquired using an intensified charge coupled device (CCD) camera for the primary instrument and a thinned, backside-illuminated CCD for the secondary instrument. The camera used in the primary instrument (developed at the Max-Planck-Institut für Aeronomie in cooperation with von Hoerner und Sulger, Schwetzingen, Germany) has a phosphor-coated expanding fiber-optics taper at the front end, which is pressed against a proximity-focused image intensifier that in turn feeds a CCD sensor having

$2K \times 2K$ pixels; the 14 μm pixels correspond to 1 arc sec resolution elements in the focal plane. (The fiber-optic taper results in an “effective” pixel size of 12 μm .) The secondary instrument uses a $1K \times 1K$ back-illuminated CCD (model SI-003A, Scientific Imaging Technologies, Tigard, OR), with each 24 μm pixel corresponding to 2 arc sec resolution elements in the focal plane.

Both instruments utilize thin, large area Al filters (150 nm) intended to minimize spectral contamination. In each case, two such filters are used in series, one at the entrance aperture and another located at the CCD camera. The larger entrance filter for the primary instrument is 10.8 cm in diameter, while all the other filters are 3.8 cm in diameter.

The optical systems of both the primary and secondary instruments are mounted to an aluminum optical bench, which is in turn mounted to the 55-cm-diameter cylindrical (aluminum) rocket skin that also acts as the vacuum vessel. The system is evacuated using a turbopump with a liquid nitrogen cold trap, and achieves a base pressure of 10^{-5} Torr after 24 h of pumping. The CCD cameras are attached to a cooling block through which liquid nitrogen is pumped prior to launch; this block also acts as a cold trap, reducing the pressure another order of magnitude. The entrance aperture of the instrument is sealed with a vacuum door mechanism that remains closed until the payload achieves the desired altitude during flight. Additionally, a valve is opened during ascent to further pump the payload prior to opening the vacuum door for the start of observations.

The flat turning mirrors that comprise the tunable Cowen–Golovchenko monochromator of the primary instrument are moved during observations using a computer-controlled stepping motor with an optical encoder. Each step corresponds to a 19.2 arc sec increment in incidence angle (and an increment of 0.01 nm in wavelength), more than adequate resolution given the bandwidth of the mirror coatings. The aperture wheel used for mirror selection in the secondary instrument is computer controlled as well.

III. INSTRUMENT PERFORMANCE

The XUV reflectance of each of the TXI multilayer mirrors was measured using the laser-plasma-based reflectometer described in Ref. 8. The reflectance measurements were made as a function of wavelength, at incidence angles near those used during flight. Thus the spherical mirrors were measured at 5° from normal, while the flat turning mirrors were measured at 15 angles spanning the range 34° – 48° . In the case of the spherical mirror designed for use at 24.9 nm, however, because reliable reflectometry data can only be obtained up to ~ 22.5 nm (due to limitations associated with the monochromator used in that system), that mirror was measured at 30° incidence. In all cases fits to the measured reflectance data were used to predict the response of the instruments at the actual flight incidence angles (i.e., 0° in the case of the spherical mirrors).

Shown in Fig. 2 is the net efficiency of the mirrors that comprise the primary instrument, as a function of wavelength, for the range of incidence angles on the flat mirrors indicated. The net efficiency was computed as the product of

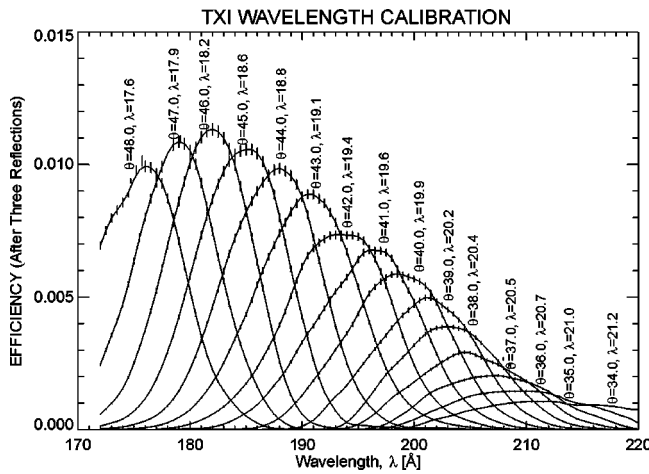
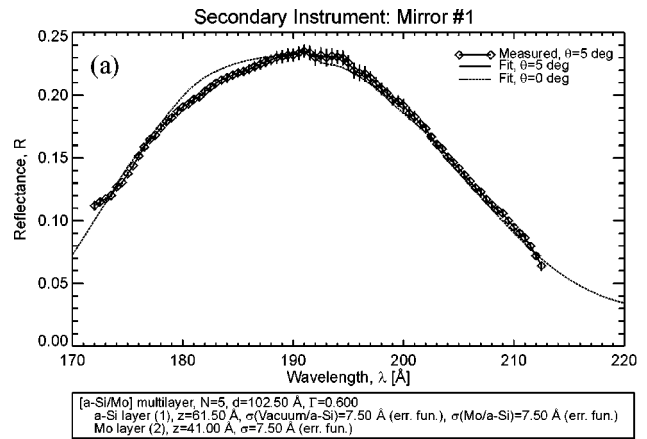


FIG. 2. Net efficiency of the three mirrors that comprise the primary TXI instrument, as a function of wavelength, for the incidence angles on the flat mirrors as indicated. The net efficiency was determined directly from the measured reflectance of the individual mirrors.

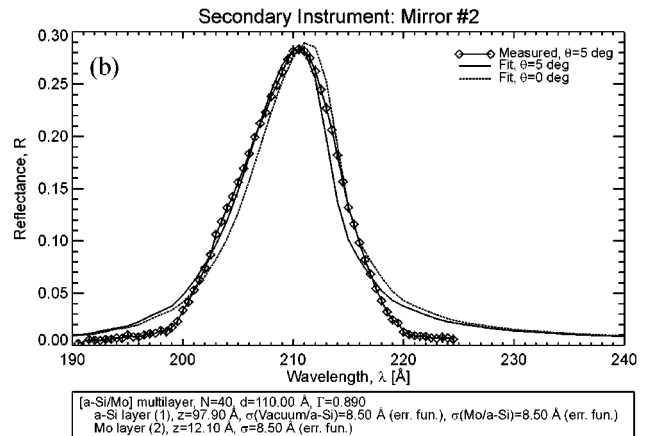
the measured reflectances obtained on each of the three mirrors, multiplied by an additional factor of 2 to account for the fact that the light striking the second flat mirror is almost completely polarized after reflecting from the first mirror at angles so close to the Brewster angle. We note that the instrument thus has strong polarization dependence: the ratio of net efficiency for *s* to *p* polarization is estimated (from fits to the reflectance data) to be $E_s/E_p \sim 10$ over the entire spectral band. The net efficiency curves shown in Fig. 2 were used to determine the relation between the incidence angle on the flat mirrors and the peak wavelength: we find $\lambda_{nm} = 29.932 - 0.254\theta_{deg}$. This relation was entered into the on-board computer that controls the flat mirror motions to allow for an accurate execution of the flight observation plan (as discussed below). Shown in Fig. 3 are the measured reflectances obtained on the three spherical mirrors that comprise the secondary instrument. The multilayer coating uniformity was also examined using reflectance measurements made at selected positions across all the mirrors. (The reflectometer beam size is $\sim 1 \text{ mm}^2$.) The uniformity variation was less than 1% in all cases, which is sufficient to avoid any significant degradation of the instrument throughput or resolution.

The efficiency of the intensified CCD detector used in the primary instrument was measured using XUV radiation generated at the BESSY synchrotron in Berlin, Germany, while the CCD used in the secondary instrument was measured at the Smithsonian Astrophysical Observatory. Quantum efficiency values at the specific wavelengths used during flight were determined by interpolation from the measured values where necessary. (We note that the detector response is fairly flat through the spectral band of the instrument.)

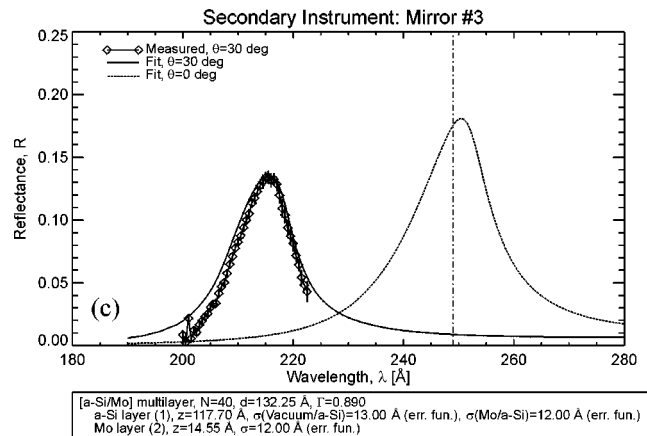
Given the measured efficiencies of the individual components that comprise the primary instrument, as just described, we estimate an effective area of $\sim 1.2 \text{ cm}^2$ at the center (peak), and 1.0 and 0.5 cm^2 at the short- and long-wavelength ends of the spectral band, respectively. The effective areas for each of the three bands that comprise the secondary instrument are similarly estimated to be $\sim 1.2 \text{ cm}^2$



[a-Si/Mo] multilayer, N=5, d=102.50 Å, $\Gamma=0.600$
 a-Si layer (1), z=61.50 Å, $\sigma(\text{Vacuum/a-Si})=7.50 \text{ \AA}$ (err. fun.), $\sigma(\text{Mo/a-Si})=7.50 \text{ \AA}$ (err. fun.)
 Mo layer (2), z=41.00 Å, $\sigma=7.50 \text{ \AA}$ (err. fun.)



[a-Si/Mo] multilayer, N=40, d=110.00 Å, $\Gamma=0.890$
 a-Si layer (1), z=97.90 Å, $\sigma(\text{Vacuum/a-Si})=8.50 \text{ \AA}$ (err. fun.), $\sigma(\text{Mo/a-Si})=8.50 \text{ \AA}$ (err. fun.)
 Mo layer (2), z=12.10 Å, $\sigma=8.50 \text{ \AA}$ (err. fun.)



[a-Si/Mo] multilayer, N=40, d=132.25 Å, $\Gamma=0.890$
 a-Si layer (1), z=117.70 Å, $\sigma(\text{Vacuum/a-Si})=13.00 \text{ \AA}$ (err. fun.), $\sigma(\text{Mo/a-Si})=12.00 \text{ \AA}$ (err. fun.)
 Mo layer (2), z=14.55 Å, $\sigma=12.00 \text{ \AA}$ (err. fun.)

FIG. 3. Measured XUV reflectance of the three mirrors that comprise the secondary TXI instrument. The measurements made at 5° incidence for mirrors No. 1 and No. 2, and at 30° for mirror No. 3 are shown along with fits to those data. The fit parameters are indicated. Also shown are the reflectance curves expected at normal incidence (0°, dotted lines), based on the fits to the measured curves.

(broadband channel), $\sim 1.3 \text{ cm}^2$ (21.1 nm channel), and $\sim 0.65 \text{ cm}^2$ (24.9 nm channel).

The TXI instrument was integrated into a Taurus-Black-Brandt sounding rocket, with pointing, telemetry, and propulsion systems provided by NASA. The rocket was launched successfully from the White Sands missile range in New Mexico on 21 June 2001 and achieved an altitude of 272 km, making possible 330 s of useful observations. The TXI primary instrument was programmed to scan in wavelength

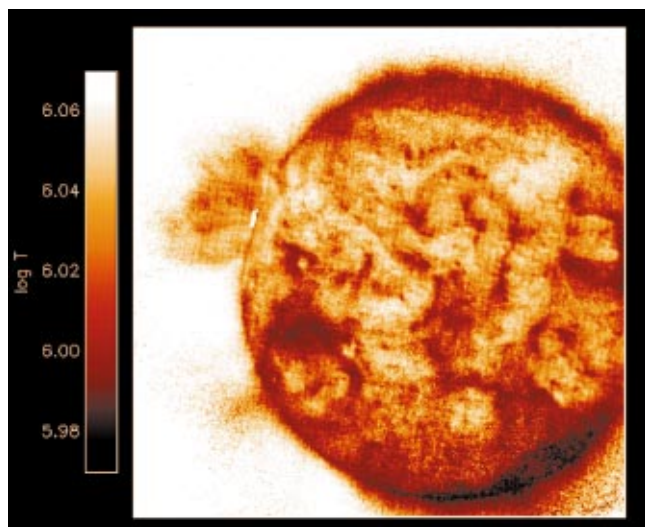


FIG. 4. (Color) Temperature map of the corona seen in the primary TXI instrument, obtained from the ratio of intensities in the 17.45 and 20.2 nm (Fe X/Fe XIII) passbands folded into a model of the coronal emission intensity as a function of plasma temperature.

from short to long and down to short again, a strategy designed to compensate for the variation in residual atmospheric extinction during flight. Thus we started at 17.45 nm, scanned to 20.4 nm, and then back down to 17.45 nm again over the course of the first 250 s. During the remaining portion of the flight a series of images was obtained at 17.45 nm, including those acquired during a 90° roll maneuver in order to make a determination of polarization in the coronal emission, thus taking advantage of the strong polarization sensitivity of this instrument (described above). The secondary instrument executed a pattern of repeated cycling through the three wavelength channels for the duration of the flight.

The data obtained from this flight will be analyzed in detail and the results will be presented elsewhere. We show here some preliminary results that demonstrate simply that both TXI instruments performed well. The first example uses data obtained with the primary TXI instrument. For plasma at a given temperature in the corona, several successive ionization states of an element such as iron are present simultaneously, in relative proportions that depend on the temperature. From a detailed model⁹ we can calculate the expected strength of the emission in the lines observed by the TXI as a function of temperature. Comparison of the changes in the relative strength of the emission in the two lines can then be interpreted as a change in temperature. To illustrate, a ratio image of Fe X/Fe XIII (17.45/20.2 nm) is shown in Fig. 4 as a temperature map. In order to determine whether or not this interpretation is valid, we plan to analyze all of the successive ionization stages and also will attempt to determine whether the same structures are visible in these different images. Nevertheless, this type of result illustrates how the unique performance characteristics of the primary TXI instrument, most notably its ability to tune continuously through a relatively wide band in the XUV containing emission lines from a number of ions, enables the construction of coronal temperature maps with high spatial resolution, and

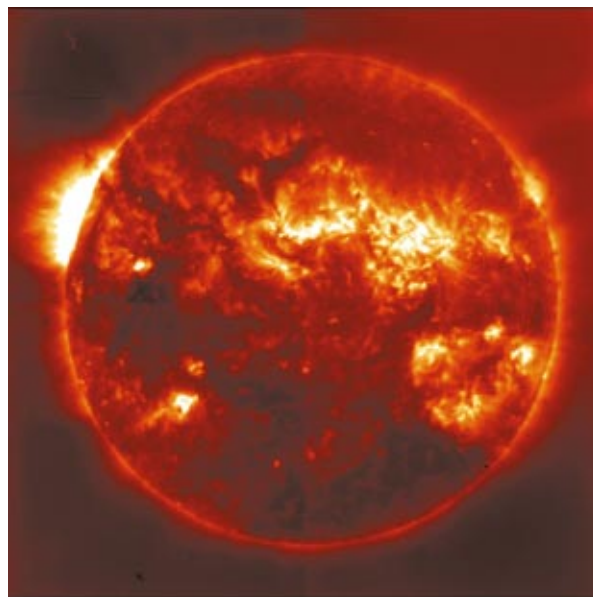


FIG. 5. (Color) Image of the solar corona obtained with one channel of the secondary TXI instrument, at $\lambda = 24.9$ nm, corresponding to emission from Ni XVII formed at $\log T = 6.5$. The solar corona has never before been imaged at this wavelength.

over the full disk of the sun, thus helping to elucidate the underlying coronal physics.

The second example, shown in Fig. 5, is an image obtained with one channel of the secondary TXI instrument, revealing the solar corona as viewed at $\lambda = 24.9$ nm. Emission from this ion (Ni XVII) provides an observation at higher plasma temperatures ($\log T = 6.5$) than have been seen at the XUV wavelengths used in previous instruments and has never before been imaged.

IV. DISCUSSION

We have described a new instrument for obtaining time-resolved, high spatial resolution images of the solar corona in the XUV band. The primary instrument is tunable continuously over the 17.1–21.1 nm wavelength band using a novel optical configuration of multilayer x-ray mirrors: the instrument consists of an $f/20$ spherical prime-focus telescope mirror coated with a broadband multilayer, in conjunction with a pair of flat mirrors coated with narrow-band multilayers arranged in a Cowen–Golovchenko double-crystal monochromator configuration. The secondary instrument uses a set of three prime-focus spherical multilayer mirrors, each tuned to specific XUV wavelength bands; the secondary instrument was designed both to supplement the primary TXI instrument wavelength coverage and to provide a test bed for new multilayer coatings and observational wavelengths.

The primary TXI instrument in particular represents a new experimental approach intended to achieve the performance requirement of isolating a narrow coronal plasma temperature interval within a wide range of plasma temperatures, as needed for useful observations of the multitemperature solar corona. The instrument performed well during its flight in June 2001. The wavelength range, although fixed for this flight, can be changed in the future simply by replacing

the mirror elements. Thus on subsequent flights we have the option of moving to other spectral regions (e.g., $25 < \lambda < 40$ nm) in order to satisfy an extended set of scientific objectives. Future flights will likely employ new multilayer coatings, containing new material combinations currently under development, that provide comparable or even better spectral resolution, while still achieving high reflectance near normal incidence (or at the larger angles used in the case of the two flat mirrors that comprise the monochromator). Higher angular resolution in the primary instrument could also be achieved in the future by increasing the fiber optic taper in the intensified CCD camera; an increase in angular resolution by a factor of 3 could be achieved easily, without the need to change any other dimensions of the optical system. The TXI concept, as demonstrated in the successful sounding rocket instrument described here, thus represents a viable approach towards achieving the performance needed for future solar physics missions that emphasize ultrahigh spatial resolution and greatly increased spectroscopic capabilities.

ACKNOWLEDGMENTS

This research was supported at the Smithsonian Astrophysical Observatory and at Columbia University by grants from NASA, and at the Max-Planck-Institut für Aeronomie by the DLR, Project No. PSAERO 456.

- ¹J. P. Delaboudinière, G. E. Artzner, J. Brunaud, A. H. Gabriel, J. F. Hochdeuz, F. Millier, X. Y. Song, B. Au, K. P. Dere, R. A. Howard, R. Kreplin, D. J. Michels, J. D. Moses, J. M. Defise, C. Jamar, P. Rochus, J. P. Chauvineau, J. P. Marioge, R. C. Catura, J. R. Lemen, L. Shing, R. A. Stern, J. B. Gurman, W. M. Neupert, A. Maucherat, F. Clette, P. Cugnon, and E. L. Van Dessel, *Sol. Phys.* **162**, 291 (1995).
- ²T. D. Tarbell, M. Bruner, B. Jurcevic, J. Lemen, K. Strong, A. Title, J. Wolfson, L. Golub, and R. Fisher, *Proceedings of the Third SOHO Workshop*, edited by V. Domingo, published by ESA Publications Division (ESTEC, Noordwijk, the Netherlands), 1994.
- ³B. N. Handy, L. W. Acton, C. C. Kankelborg, C. J. Wolfson, D. J. Akin, M. E. Bruner, R. Carvalho, R. C. Catura, R. Chevalier, D. W. Duncan, C. G. Edwards, C. N. Feinstein, S. L. Freeland, F. M. Friedlander, C. H. Hoffmann, N. E. Hurlburt, B. K. Jurcevic, N. L. Katz, G. A. Kelly, J. R. Lemen, M. Levay, R. W. Lindgren, D. P. Mathur, S. B. Meyer, S. J. Morrison, M. D. Morrison, R. W. Nightingale, T. P. Pope, R. A. Rehse, C. J. Schrijver, R. A. Shine, L. Shing, T. D. Tarbell, A. M. Title, D. D. Torgerson, L. Golub, J. A. Bookbinder, D. Caldwell, P. N. Cheimets, W. N. Davis, E. E. DeLuca, R. A. McMullen, D. Amato, R. Fisher, H. Maldonado, and C. Parkinson, *Sol. Phys.* **187**, 229 (1999); see also (<http://vestige.lmsal.com/TRACE>)
- ⁴K. P. Dere, J.-D. Bartoe, G. E. Brueckner, J. W. Cook, and D. G. Socker, *Sol. Phys.* **114**, 223 (1987).
- ⁵G. A. Linfood and C. J. Wolfson, *Astrophys. J.* **331**, 1036 (1988).
- ⁶T. Yoshida, S. Tsuneta, L. Golub, K. Strong, and Y. Ogawara, *Publ. Astron. Soc. Jpn.* **47**, L15 (1995); A. Takeda *et al.*, in *Proceedings of the IAU Symposium 153*, edited by Y. Uchida, T. Kosugi, and H. S. Hudson (Kluwer, Dordrecht, 1995); A. B. C. Walker, R. B. Hoover, and T. W. Barbee, Jr., in *Physics of Solar and Stellar Coronae*, edited by J. Linsky and S. Serio (Kluwer, Dordrecht, 1993), p. 97.
- ⁷P. L. Cowan, T. J. Hasting, and J. P. Kirkland, *Nucl. Instrum. Methods Phys. Res.* **208**, 349 (1983).
- ⁸D. L. Windt and W. K. Waskiewicz, *J. Vac. Sci. Technol. B* **12**, 3826 (1994).
- ⁹K. P. Dere, E. Landi, H. E. Mason, B. C. Monsignori Fossi, and P. R. Young, *Astron. Astrophys.* **125**, 149 (1997).